Materials Transactions, Vol. 43, No. 8 (2002) pp. 1966 to 1973
Special Issue on Bulk Amorphous, Nano-Crystalline and Nano-Quasicrystalline Alloys IV

Magnetic Properties and Phase Transformations of Bulk Amorphous Fe-Based Alloys Obtained by Different Techniques

Mihai Stoica[1], Jarmila Degmová[1,4], Stefan Roth[1], Jürgen Eckert[1], Helgard Grahl[1], Ludwig Schultz[1], Alain Reza Yavari[2], Åke Kvick[3] and Guido Heunen[3]

[1]*IFW Dresden, Institute for Metallic Materials, P. O. Box 270016, D-01171 Dresden, Germany*
[2]*LTPCM (CNRS umr 5614), Institut National Polytechnique de Grenoble, BP 75, 38402 St-Martin-d'Hères Campus, France*
[3]*European Synchrotron Radiation Facilities ESRF, 38042 Grenoble, France*
[4]*Department of Nuclear Physics and Technology, Slovak University of Technology, Ilkovicova 3, 81219 Bratislava, Slovakia*

Bulk amorphous $Fe_{65.5}Cr_4Mo_4Ga_4P_{12}C_5B_{5.5}$ rods with diameters of 1.5–3 mm were prepared by copper mold casting. Besides casting, bulk amorphous $Fe_{77}Al_{2.14}Ga_{0.86}P_{8.4}C_5B_4Si_{2.6}$ samples in the shape of discs (diameter of 10 mm and thickness of 3 mm) were prepared from melt-spun ribbons by high-energy ball milling and subsequent compaction of the resulting powders in the supercooled liquid region. The as-cast amorphous FeCrMoGaPCB samples exhibit a low coercivity, below 10 $A{\cdot}m^{-1}$. In the case of the FeAlGaPCBSi alloy, the milling-induced stress causes significant differences in coercivity between the ribbons and the powders. The relatively low coercivity of about 5–10 $A{\cdot}m^{-1}$ characteristic for the melt-spun ribbons increases after 1 hour of ball milling to a value of about 2200 $A{\cdot}m^{-1}$. Subsequent annealing of the ball-milled powders leads to a decrease of H_c by a factor of 10 to about 220–250 $A{\cdot}m^{-1}$. The bulk samples prepared by hot pressing of the crushed ribbons show a coercivity of about 120–140 $A{\cdot}m^{-1}$. For both alloys, thermal stability measurements show a distinct glass transition, followed by a supercooled liquid region of 60 K for $Fe_{65.5}Cr_4Mo_4Ga_4P_{12}C_5B_{5.5}$ and of 30 K for $Fe_{77}Al_{2.14}Ga_{0.86}P_{8.4}C_5B_4Si_{2.6}$. For the $Fe_{65.5}Cr_4Mo_4Ga_4P_{12}C_5B_{5.5}$ alloy, crystallization of the amorphous phase as observed by *in-situ* X-ray diffraction measurements in transmission configuration occurs via the formation of a metastable intermediate phase. The phases observed in the crystalline state obtained by heating do not correspond to those occurring after slow cooling.

(Received February 25, 2002; Accepted April 15, 2002)

Keywords: *iron-based alloys, melt-spun ribbons, ball-milled powders, supercooled-liquid region, coercivity, hot pressing, amorphous rods*

1. Introduction

The Fe-based amorphous alloys recently found by Inoue *et al.*[1–5] exhibit a large supercooled liquid region between the glass transition temperature T_g and the crystallization temperature T_x visible upon constant-rate heating to elevated temperatures. Because of the lack of crystalline anisotropy, they have good soft magnetic properties characterized by low coercive force and high permeability.[6–9] Nevertheless, residual anisotropy may be present, such as shape anisotropy or stress-induced anisotropy caused by internal mechanical stress induced by the preparation procedure, *i.e.* rapid quenching, slow cooling[9,10] or ball milling.[11] The high glass-forming ability of this kind of alloys allows the formation of bulk glassy samples.[12] However, the critical cooling rate of about 10^2 $K{\cdot}s^{-1}$ required for glass formation of these alloys limits the diameter of the samples.[13] The other hindrance that can influence bulk glass formation is the presence of impurities in the melt.[14,15] When the conditions for glass formation are met (*e.g.* low impurity content, *etc.*) such alloys can be directly cast in form of bulk specimens, which could be used for magnetic cores. Inoue and co-workers[16] reported that for FeAlGaPCBSi alloys ribbons with dimensions of up to 0.015 mm × 0.5 mm and cylinders up to a diameter of 3 mm can be prepared by melt spinning and copper mold casting, respectively. In the case of FeCrMoGaPCB alloys, Shen and Schwarz[15] used the flux-melting technique to remove the oxide inclusions from the melt and subsequent water quenching allows to produce rods with 4 mm diameter. The critical cooling rate of about 10^2 $K{\cdot}s^{-1}$ is higher compared to the value of about 1–10 $K{\cdot}s^{-1}$ characteristic for the alloys with very good glass-forming ability.[17,18] Thus, in order to prepare amorphous samples with good soft magnetic properties the maximum achievable diameter (in the case of copper mold casting) is limited to a few millimetres.

On the other hand, bulk amorphous samples with various sizes and shapes can be prepared by mechanical alloying or ball milling combined with subsequent consolidation of the resulting powders in the viscous state at temperatures in the supercooled liquid region.[19,20] High-energy ball milling induces stresses, which can be successfully reduced by annealing the resulting powders at temperatures below the onset of crystallization.[11,21] The enhanced coercivity of annealed ball milled powders in comparison with melt-spun ribbons is supposed to be mainly caused by presence of nonmagnetic oxide phases formed during milling on the reactive surface of the powder particles.[11] The consolidation process can be combined with annealing in the supercooled liquid region in order to obtain bulk specimens with amorphous structure. This can yield bulk amorphous specimens with larger dimensions than those achievable by slow cooling from the melt.[22]

Both amorphous alloys, $Fe_{65.5}Cr_4Mo_4Ga_4P_{12}C_5B_{5.5}$ and $Fe_{77}Al_{2.14}Ga_{0.86}P_{8.4}C_5B_4Si_{2.6}$, have soft magnetic properties. The first one can be produced directly in rod form by copper mold casting, but the maximum diameter where the alloy is fully amorphous is limited to about 3–4 mm.[3] The coercivity is below 10 $A{\cdot}m^{-1}$ and is influenced by crystalline inclusions, and the saturation polarization is around 0.8 T.[15] Besides that, the $Fe_{77}Al_{2.14}Ga_{0.86}P_{8.4}C_5B_4Si_{2.6}$ bulk amorphous alloys obtained by ball milling of amorphous ribbons and sub-

sequent consolidation in form of discs with 10 mm diameter and different thickness exhibit a coercivity which is one order of magnitude higher compared to the as-spun amorphous ribbon, but it can be decreased by annealing. Hence, not only the alloy composition but also the processing route have a strong influence on glass formation as well as on the resulting soft magnetic properties of the material. This also holds for the possibility to produce bulk amorphous Fe-based alloys in shapes suitable for magnetic applications. Consequently, this work focuses on the crystallization behavior, the magnetic properties for $Fe_{65.5}Cr_4Mo_4Ga_4P_{12}C_5B_{5.5}$ and $Fe_{77}Al_{2.14}Ga_{0.86}P_{8.4}C_5B_4Si_{2.6}$ bulk glass-forming alloys prepared by slow cooling from the melt or by melt spinning combined with crushing of the ribbons by ball milling and subsequent consolidation.

2. Experimental Procedure

The preparation of the amorphous $Fe_{65.5}Cr_4Mo_4Ga_4P_{12}C_5B_{5.5}$ and $Fe_{77}Al_{2.14}Ga_{0.86}P_{8.4}C_5B_4Si_{2.6}$ alloys was done in several steps. First, master alloy ingots were obtained by induction melting using Fe–B, Fe–C, Fe–Ga, Fe–P prealloys and pure elements like Mo (99.4% purity), Cr (99.95% purity), Fe (99.9% purity), Al (99.95% purity), Si (99.99% purity) or crystalline B (99.99% purity). Induction melting of Fe with B, Fe with C (99.9% purity) and Fe with Ga (99.7% purity) allowed to produce the respective pre-alloys. By mechanical alloying of Fe powder (99.9% purity, less than 10 microns particle size) with amorphous red P (99% purity, less than 100 microns particle size) in SPEX 8000 ball mill using hardened steel balls and vial and a 3:1 ball-to-powder weight ratio, consolidation of the resulting powders by cold pressing and subsequent induction melting the pre-alloy, was obtained the Fe–P pre-alloy. The handling of the elements, the ball milling as well as the powder, compaction and the melting were performed under protective atmosphere (argon, purity 99.99%).

Amorphous rods (diameter of 1.5, 2, 2.5 and 3 mm, length of 70 mm) and ribbons (width of 10 mm and thickness of 0.03 mm) were prepared from the master alloy with nominal composition $Fe_{65.5}Cr_4Mo_4Ga_4P_{12}C_5B_{5.5}$. The rods were obtained by induction melting under argon atmosphere at a pressure of 80 kPa and subsequent injection into a cylindrical copper mold under an applied pressure of $3{\cdot}10^5$ Pa. The amorphous ribbons were prepared by single-roller melt spinning on a copper wheel under argon flow at $24\,m{\cdot}s^{-1}$ tangential velocity of the wheel. Using the same device, $Fe_{77}Al_{2.14}Ga_{0.86}P_{8.4}C_5B_4Si_{2.6}$ amorphous ribbons of 10 mm in width and 0.02 mm in thickness were prepared using a wheel speed of $21\,m{\cdot}s^{-1}$. Some parts of these ribbons were cut into small pieces, ball-milled and subsequently compacted to discs of 10 mm in diameter and 3 mm in thickness. The milling experiments were done in a Retsch PM 4000 planetary ball mill under an argon atmosphere using hardened steel balls and vials and the ball-to-powder weight ratio was 15:1. The rotation velocity of the mill was 250 revolutions per minute. The sample handling was performed in a glove box under purified argon atmosphere (<1 ppm O_2 and H_2O). The consolidation of the resulting powders into bulk samples was done in an unaxial hot press under a vacuum of 10^{-3} Pa. The powder was heated at $0.67\,K{\cdot}s^{-1}$ to the consolidation temperature, held isothermally at this temperature and compacted at a pressure of 500 MPa. The sample was held isothermally in the press under the applied load for 2 min. The compacting temperatures were chosen to be in the temperature range of the supercooled liquid region. The oxygen content of the powders after milling was checked by hot extraction using a C436 LECO analyser. Because the presence of oxides can have a negative influence in order to prepare bulk amorphous alloys, we also checked the oxygen content of the master alloys and prealloys. This revealed very low values: 50 ppm for $Fe_{65.5}Cr_4Mo_4Ga_4P_{12}C_5B_{5.5}$ and $Fe_{77}Al_{2.14}Ga_{0.86}P_{8.4}C_5B_4Si_{2.6}$, 180 ppm for Fe–P and 130 ppm for the other pre-alloys, respectively.

The amorphous structure of the samples was checked by X-ray diffraction (XRD) experiments with Co–Kα radiation ($\lambda = 0.17889$ nm) using a Phillips PW 3020 diffractometer. Because the diameter of the $Fe_{65.5}Cr_4Mo_4Ga_4P_{12}C_5B_{5.5}$ rods was rather small, the samples for XRD measurements were prepared by crushing the rods into small pieces and bonded into amorphous resin in order to have good resolution. The thermal stability, *i.e.* the glass transition, the extension of the supercooled liquid region and the crystallization, was examined by differential scanning calorimetry (DSC), using a Netzsch DSC 404 for $Fe_{65.5}Cr_4Mo_4Ga_4P_{12}C_5B_{5.5}$ amorphous ribbons and rods and a Perkin-Elmer DSC 7 for $Fe_{77}Al_{2.14}Ga_{0.86}P_{8.4}C_5B_4Si_{2.6}$ amorphous ribbons and compacted samples. The glass transition temperature T_g and the crystallization temperature T_x were measured as the onset temperatures of the glass transition and the crystallization events, respectively, during heating with a constant rate of $0.67\,K{\cdot}s^{-1}$. The extension of the supercooled liquid region, defined as the difference between the glass transition temperature and the crystallization temperature, $\Delta T_x = T_x - T_g$ was also calculated. Additionally, for the $Fe_{65.5}Cr_4Mo_4Ga_4P_{12}C_5B_{5.5}$ alloy the melting temperature T_m defined by the liquidus temperature T_{liq} at the onset of solidification upon cooling with a constant rate of $0.17\,K{\cdot}s^{-1}$ was measured using the Netsch DSC 404.

For $Fe_{77}Al_{2.14}Ga_{0.86}P_{8.4}C_5B_4Si_{2.6}$ amorphous alloys, penetration measurements in the supercooled liquid region were carried out by parallel plate rheometry in a Perkin-Elmer TMA7 analyser with quartz penetration probe as parallel plates in an argon atmosphere at a heating rate of $0.67\,K{\cdot}s^{-1}$. The applied static force was 2.6 N. The isothermal annealing experiments were done in a tin-bath furnace.

The crystallization behavior during heating and subsequent cooling from the melt of glassy $Fe_{65.5}Cr_4Mo_4Ga_4P_{12}C_5B_{5.5}$ rods were observed by *in-situ* X-ray diffraction measurements in transmission configuration, using a high intensity high-energy monochromatic synchrotron beam ($\lambda = 0.01304$ nm) at the ESRF Grenoble. The rods were cut into pieces of 15 mm length and sealed into fused silica tubes under a vacuum of 10^{-3} Pa. The as-prepared samples were fast induction-heated with a rate of $2–5\,K{\cdot}s^{-1}$ up to the melting point, overheated and cooled down with $20\,K{\cdot}s^{-1}$, *i.e.* a cooling rate not sufficient to retain an amorphous phase, with acquisition of X-ray patterns at each 2 s during the all process.

The magnetic properties of the samples were also investigated. The coercive force, H_c, was measured using a Foerster

Koerzimat with premagnetizing field pulses of 2000 A·cm^{-1}, the saturation polarization, J_s, was measured by a vibrating sample magnetometer (VSM) under a maximum DC magnetic field of 15000 A·cm^{-1} and the behavior of magnetization versus applied magnetic field was determined by a *B–H* loop tracer which allows a continuous variation of the magnetic field between −200 and 200 A·cm^{-1}.

3. Results and Discussion

3.1 Bulk amorphous $Fe_{65.5}Cr_4Mo_4Ga_4P_{12}C_5B_{5.5}$ rods and ribbon

3.1.1 Thermal characterization

The thermal stability of amorphous $Fe_{65.5}Cr_4Mo_4Ga_4P_{12}C_5B_{5.5}$ rods prepared by copper mold casting is shown in Fig. 1. The DSC scans reveal a glass transition starting at T_g, followed by a distinct supercooled liquid region and crystallization starting at T_x (the onset temperatures of glass transition and crystallization are marked by arrows in the figure). The values for T_g, T_x and $\Delta T_x = T_x - T_g$ for the different specimens are summarized in Table 1, together with the melting temperatures T_m, measured as the onset of solidification upon cooling. We used these temperatures to calculate the ratio T_g/T_m. Its value of about 0.59 is characteristic for alloy systems with good glass forming ability.[18,23] The glass transition temperature and the crystallization temperature increase slowly with increasing rod diameter, whereas the extension of the supercooled liquid region $\Delta T_x = 60 \pm 1$ K remains almost constant. For the ribbon, $\Delta T_x = 66$ K and the glass transition starts at 743 K, *i.e.* about 10 ± 3 K earlier in comparison with the rods (750 K for the rod with 1.5 mm diameter or 757 K for the rod with 3 mm in diameter, respectively). The glass transition temperature, as well as the crystallization temperature, increase monotonically with increasing diameter of the rods, and their values are about 30 K higher than the data reported by Shen and Schwarz[15] for this type of Fe-based bulk amorphous alloys obtained by water quenching.

These differences in thermal stability between the melt-spun ribbons and the rods of different diameter cannot be attributed simply to a different degree of relaxation obtained by the different cooling rates realized during melt spinning and copper mold casting. Rather they point to slightly different actual compositions of the glass obtained by the different synthesis conditions and the decreasing cooling rate of the melt with increasing diameter of the rods. Such compositional variations may arise if at least the rods with larger diameter are not fully amorphous but contain some crystalline primary precipitates wich may form due to not sufficient cooling rate for complete glass formation upon casting.

3.1.2 Structural characterization

The XRD patterns ($\lambda = 0.17889$ nm), taken in the reflection configuration for crushed as-cast samples, are presented in Fig. 2. Generally, the patterns display a broad maximum centered around $2\theta = 51°$ which is characteristic for an amorphous phase. However, the XRD experiments do not rule out the possible existence of a small volume fraction of nanoscale crystalline precipitates, which may be present in the glassy matrix. For example, there are additional diffraction peaks with weak intensity superimposed on the broad diffraction maximum of the amorphous phase for the cast rod with 3 mm diameter (curve d in Fig. 2). This points to the formation of crystalline precipitates coexisting with the glass, which agrees well with the conclusions drawn from the DSC results.

The X-ray diffraction measurements in transmission configuration, using a high intensity high-energy monochromatic synchrotron beam ($\lambda = 0.01304$ nm) at the ESRF Grenoble showed clearly the presence of another crystalline phase(s) coexisting with the amorphous matrix. Figure 3 presents a comparison of patterns taken in this geometry, for the fully amorphous as-cast 1.5 mm rod and for the as-cast 3 mm rod with precipitates. The fully amorphous sample exhibits only two broad diffraction maxima centered around 31 nm^{-1} and 53 nm^{-1}, respectively. The first peak centered around of 15 nm^{-1} corresponds to the sample holder. In contrast, the XRD pattern for the 3 mm diameter rod (curve b in Fig. 3)

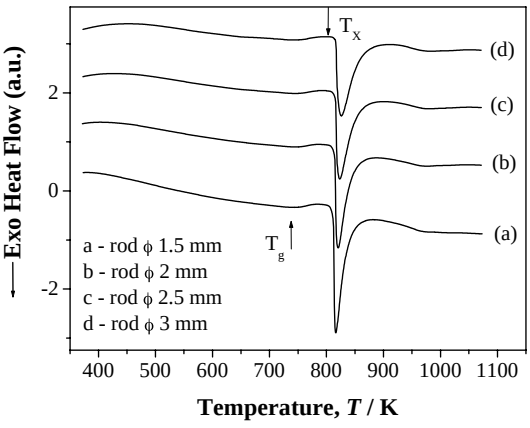

Fig. 1 The DSC curves measured at a heating rate of 0.67 K·s^{-1} for amorphous $Fe_{65.5}Cr_4Mo_4Ga_4P_{12}C_5B_{5.5}$ samples with different thickness.

Table 1 Thermal stability data for $Fe_{65.5}Cr_4Mo_4Ga_4P_{12}C_5B_{5.5}$ glassy alloys with different thickness measured at 0.67 K·s^{-1} heating rate.

Sample	T_g/K	T_x/K	ΔT_x/K	T_m/K	T_g/T_m
Ribbon	743	809	66	1256	0.59
Rod ϕ 1.5 mm	750	811	61	1251	0.59
Rod ϕ 2 mm	753	814	61	1248	0.60
Rod ϕ 2.5 mm	755	815	60	1250	0.60
Rod ϕ 3 mm	757	817	60	1251	0.60

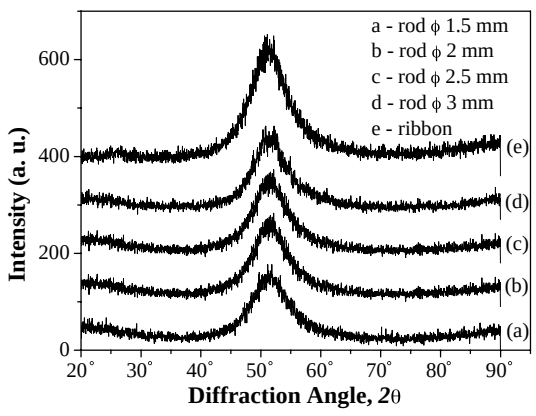

Fig. 2 XRD scans for bulk amorphous $Fe_{65.5}Cr_4Mo_4Ga_4P_{12}C_5B_{5.5}$ as-cast rods and ribbon.

displays additional diffraction peaks at 43.9, 51.6, 53.1, 56.8, 59.5, 61.9 and 68.9 nm^{-1}, respectively. This clearly proves the presence of crystalline inclusions in this specimen. The peaks with the wave vectors Q of 43.9, 53.1, 61.9 and 68.9 nm^{-1} correspond to the *bcc* phase characteristic for α-Fe. The other peaks at 51.6, 56.8 and 59.5 nm^{-1} are characteristic for a Fe_3C-type structure. Scanning electron microscopy (SEM) images taken from the cross-section of the as-cast 3 mm diameter rod (not showed here) reveal a dendritic structure for the crystalline inclusions with a dendrite size of 60–70 μm. Most likely, the crystals form by primary precipitation upon cooling from the melt.

Figure 4 shows the XRD patterns recorded in transmission geometry, for the as-cast 3 mm rod taken at different temperatures, *i.e.* for the as-cast material at room temperature, in the molten state at 1448 K and during cooling at 1313 K, where the alloy is still melted but may contain some clusters/inclusions (according to the DSC measurements the melting temperature is around 1251 K-see Table 1). In the molten state at 1313 K as well as at room temperature (Figs. 4(a) and (c)), there appears the same crystalline Fe_3C-type phase besides the amorphous phase. Obviously, the casting temperature plays an important role for obtaining a completely amorphous alloy. The alloy must be overheated until all the clusters/inclusions are melted (curve b in Fig. 4). Judging from the *in-situ* XRD measurements, the optimum casting temperature is around 200 K above the liquidus temperature, and at the same time must not be too high in order to retain a proper cooling rate.

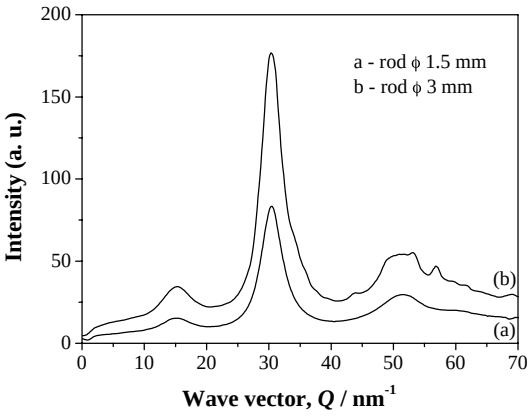

Fig. 3 Transmission XRD patterns of glassy $Fe_{65.5}Cr_4Mo_4Ga_4P_{12}C_5B_{5.5}$ alloys for: (a) a rod with 1.5 mm diameter and (b) a rod with 3 mm diameter, respectively.

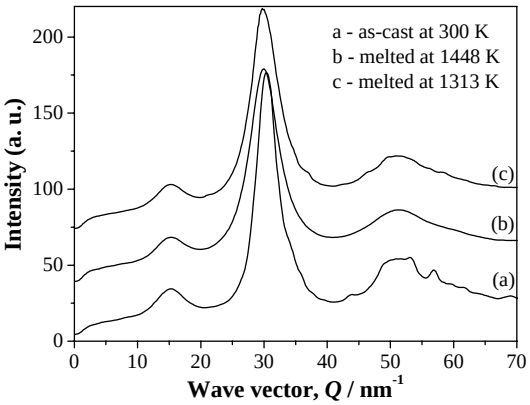

Fig. 4 Transmission XRD patterns of glassy $Fe_{65.5}Cr_4Mo_4Ga_4P_{12}C_5B_{5.5}$ alloys recorded *in-situ* at different temperatures: (a) at room temperature, (b) melted at 1448 K and (c) melted at 1313 K.

The XRD patterns for the 2.5 mm in diameter sample taken *in-situ* during heating with a rate of 5 $K \cdot s^{-1}$, melting above T_{liq} and subsequent cooling with 20 $K \cdot s^{-1}$ are presented in Fig. 5. The successive patterns correspond to different temperatures, starting from the amorphous phase at room temperature, crystallized above T_x, melted, overheated and crystallized after fast cooling. The sample consists of a single amorphous phase at room temperature (curve a in Fig. 5). At 1013 K (curve b), the sample is completely crystalline. The peaks correspond to *bcc* α-Fe, *fcc* γ-Fe and Fe_3C-type structure. Above this temperature, the peaks corresponding to *fcc* γ-Fe (curve c) prevail. Besides, intermetallic compounds of the form $(Fe, Cr, Mo, Ga)_x(P, B, C)_{100-x}$ may form, which have not been clearly identified, yet. At 1488 K, the crystalline structure disappears completely and all the clusters/inclusions are completely melted (curve d). The curve e in Fig. 5 corresponds to the crystalline state formed after cooling. The pattern is similar to that shown in curve c, and corresponds mainly to *fcc* γ-Fe phase, which is probably due to the retention of the austenitic phase by carbon. The peaks corresponding to the Q wave vector for the Fe_3C-type structure do not match the relative distribution of the peak intensity. For clarity, in the patterns presented in Fig. 5 only the peaks corresponding to *bcc* α-Fe and *fcc* γ-Fe are marked.

3.1.3 Magnetic measurements

Table 2 summarizes the values of the coercive force H_c and of the saturation polarization J_s for as-cast amorphous rib-

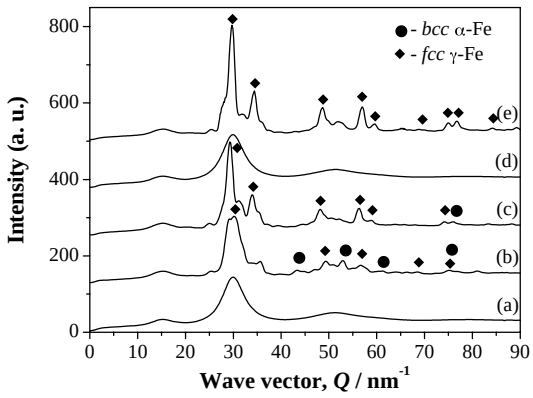

Fig. 5 The crystallization of amorphous $Fe_{65.5}Cr_4Mo_4Ga_4P_{12}C_5B_{5.5}$ investigated by *in-situ* measurements for a rod with a diameter of 2.5 mm: (a) at room temperature, (b) at 1013 K, (c) at 1273 K, (d) overheated to 1488 K and (e) crystalline at room temperature after cooling.

Table 2 Magnetic data for $Fe_{65.5}Cr_4Mo_4Ga_4P_{12}C_5B_{5.5}$ glassy alloys with different thickness.

Sample	Coercivity H_c/A·m^{-1}	Saturation polarization J_s/T
Ribbon	1.7	0.82
Rod ϕ 1.5 mm	5	0.81
Rod ϕ 2 mm	3	0.77
Rod ϕ 2.5 mm	9	0.78
Rod ϕ 3 mm	62	0.78

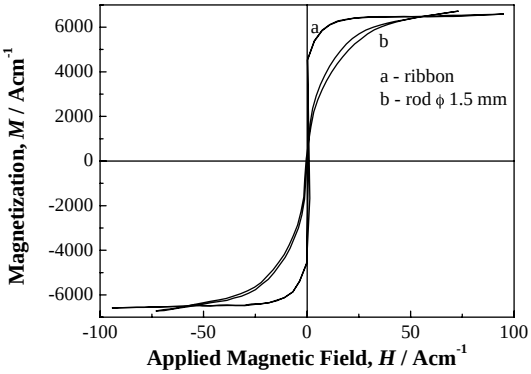

Fig. 6 The M–H loops for as-cast amorphous $Fe_{65.5}Cr_4Mo_4Ga_4P_{12}C_5B_{5.5}$ samples with different diameters: (a) 1.5 mm and (b) 2 mm.

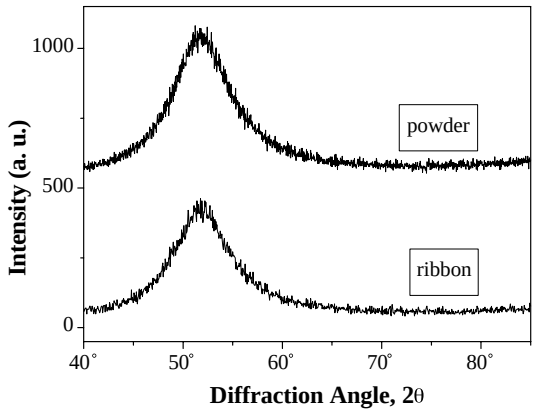

Fig. 7 XRD patterns for $Fe_{77}Al_{2.14}Ga_{0.86}P_{8.4}C_5B_4Si_{2.6}$ ribbon and ball-milled powder.

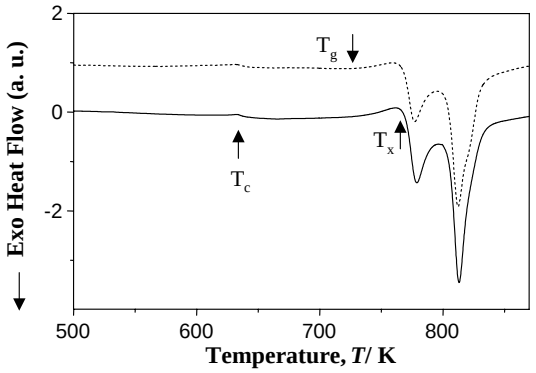

Fig. 8 DSC curves for $Fe_{77}Al_{2.14}Ga_{0.86}P_{8.4}C_5B_4Si_{2.6}$ melt-spun ribbon (solid line) and ball-milled powder (dotted line) taken at a heating rate 0.67 K·s^{-1}. The characteristic temperatures T_g and T_x are also indicated. The small endothermic reaction at about 630 K is attributed to the Curie temperature T_c.

bons and rods without crystalline inclusions. The values are different for samples with different shape or diameter. The lowest coercivity value of 1.7 A·m^{-1} is found for the ribbon and the coercivity increase to 9 A·m^{-1} for the 2.5 mm diameter rod. However, the coercivity does not increase monotonically with increasing diameter of the rods, *i.e.* does not depend on the geometry of the sample, but is probably most sensitive to residual stress induced during the casting and to crystalline inclusions. For the as-cast rod with 3 mm diameter, which is not fully amorphous, the coercivity increases to 62 A·m^{-1} and it is expected to depend on the volume fraction of crystalline inclusions. The values of the saturation polarization are in the range of 0.77–0.82 T for the as-cast samples and were calculated using the estimated density value of 7057 kg·m^{-3}. The values are of the same order as the reported literature data for this type of amorphous alloys.[15] Figure 6 presents a comparison of the M–H hysteresis loops for an amorphous rod with 1.5 mm diameter and a ribbon for an maximum applied field of 100 A·cm^{-1}. The magnetization at 80 A·cm^{-1} for both sample are near the same value around 6200 A·cm^{-1}, which correspond to a value of 0.77 T for polarization. The main errors that appear during the magnetic determination are due to the difficulties to estimate precisely the rather small cross-section of the ribbon.

3.2 Bulk amorphous $Fe_{77}Al_{2.14}Ga_{0.86}P_{8.4}C_5B_4Si_{2.6}$ discs

3.2.1 Milling induced changes of thermal, structural and magnetic properties

In order to prepare bulk amorphous samples, in a first step melt spinning was used to produce amorphous $Fe_{77}Al_{2.14}Ga_{0.86}P_{8.4}C_5B_4Si_{2.6}$ ribbons which were then crushed into small pieces and subsequently ball-milled. The process of ball milling induces internal mechanical stress in the material and produces surface roughness. Accordingly, the thermal, structural and magnetic properties of the resulting powder are different from those of the initial melt-spun ribbon.

Figure 7 compares the X-ray diffraction patterns for the ribbon and for the 1 h ball-milled powder. In both cases only the diffuse halo typical for an amorphous phase and no peaks for crystalline phases are found. Thus, one can suppose that no massive crystallization occurs during milling.

The width of the temperature region ΔT_x during which the sample is in the supercooled liquid state is influenced by ball-milling. Figure 8 shows DSC curves recorded at a heating rate 0.67 K·s^{-1} for $Fe_{77}Al_{2.14}Ga_{0.86}P_{8.4}C_5B_4Si_{2.6}$ melt-spun ribbon and ball-milled powder. For the ribbon, the supercooled liquid region spreads over about 40 K ($T_g \approx 732$ K, $T_x \approx 772$ K), whereas $\Delta T_x = 35$ K ($T_g \approx 733$ K, $T_x \approx 768$ K) in the case of the powder. This is due to the increase of the oxygen content upon ball milling which promotes crystallization of the powder.[24,25] The initial ribbon reveals an oxygen content of 0.04 ± 0.01 at%, whereas the ball-milled powder contains about 0.08 ± 0.01 at% of oxygen. Hence, after ball milling for 1 h the oxygen content doubled.

The limiting values of the ΔT_x temperature region are important for compaction because of the material softening which starts at temperatures above T_g. Figure 9 shows the penetration for $Fe_{77}Al_{2.14}Ga_{0.86}P_{8.4}C_5B_4Si_{2.6}$ ribbon and ball-milled powder as a function of temperature recorded in the Perkin-Elmer TMA7 analyser at a constant heating rate 0.67 K·s^{-1}. Above glass transition temperature the distinct contraction of the sample (*i.e.* penetration of the probe) occurs due to decrease of the viscosity in this temperature region. The diminution of the viscosity in the supercooled liquid state allows to consolidate dense bulk samples because of the easy deformation and working processes in this region.[26,27]

The ball milling-induced stress causes significant differences in coercivity (H_c) between the melt-spun ribbon and

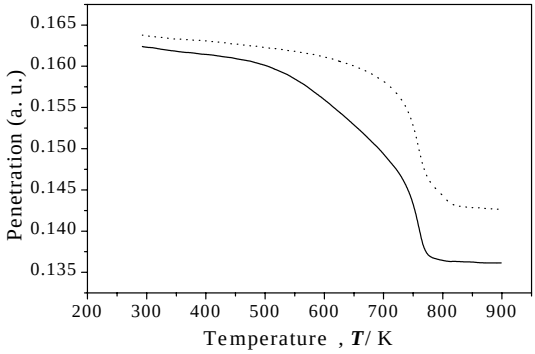

Fig. 9 TMA scan of $Fe_{77}Al_{2.14}Ga_{0.86}P_{8.4}C_5B_4Si_{2.6}$ ribbon (solid line) and ball-milled powder (dotted line) as the functions of temperature recorded at a constant heating rate of $0.67\,K{\cdot}s^{-1}$.

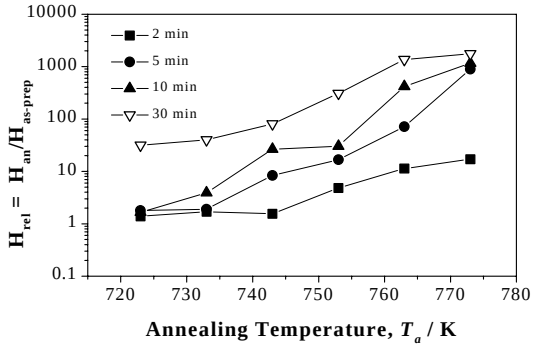

Fig. 10 Coercive force of $Fe_{77}Al_{2.14}Ga_{0.86}P_{8.4}C_5B_4Si_{2.6}$ ribbon as a function of annealing temperature T_a for different annealing times (2, 5, 10 and 30 min).

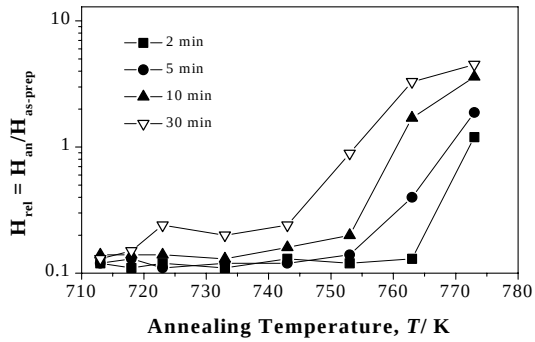

Fig. 11 Coercive force of $Fe_{77}Al_{2.14}Ga_{0.86}P_{8.4}C_5B_4Si_{2.6}$ powder as a function of annealing temperature T_a for different annealing times (2, 5, 10 and 30 min).

the ball-milled powder. After melt-spinning a relatively low coercivity of 5–10 $A{\cdot}m^{-1}$ is found, which is typical for as-quenched ribbons.[2)] The coercivity increases strongly even after short ball milling for 1 h to a value of about 2200 $A{\cdot}m^{-1}$. This increase of H_c values after ball milling can be attributed to microstructural changes (as a contribution of surface irregularities *etc.*) of the amorphous material induced by the milling process.[21)] Mechanical treatment of $Fe_{77}Al_{2.14}Ga_{0.86}P_{8.4}C_5B_4Si_{2.6}$ amorphous material affects its soft magnetic properties and causes an increase of coercivity, similar as it was shown for mechanically alloyed Fe-TM-based alloys.[28)] It was found that in the early stage of ball milling of an amorphous phase, shear bands are formed which hinder the domain wall motion.[21)] In the case of low oxygen content in ball-milled powder, the pinning of domain walls at oxides as the reason for increased coercivity can be excluded.[21)] A large coercivity relaxation of ball-milled powder is obtained by annealing at elevated temperatures which will be discussed in the next section.

3.2.2 Annealing experiments

The coercivity of ribbon and powder can be changed by annealing at elevated temperatures. Figures 10 and 11 show the changes of coercivity for the ribbon and the ball-milled powder obtained by annealing at elevated temperatures (T_a) for four different times (2, 5, 10 and 30 minutes) and 7 different temperatures ranging from 713 K up to 773 K. Annealing of the ribbons for 2 min does not significantly change the H_c values for temperatures up to $T_a = 743$ K. 30 minutes of annealing at 723 K increases H_c by one order of magnitude: from 5–10 $A{\cdot}m^{-1}$ ($= H_{as-prep}$) to 96 $A{\cdot}m^{-1}$. This indicates the presence of some crystals in the sample. Annealing at 763 K (which is close to T_x) for 30 minutes leads to an increase of H_c to 8155 $A{\cdot}m^{-1}$, which reveals a rather advanced crystallization of the sample. Finally, at this temperature even a short annealing for 2 minutes causes a H_c increase by about one order of magnitude from 5 to 70 $A{\cdot}m^{-1}$.

In the case of powder one observes a different behaviour. Annealing of ball-milled powder for 2 and 5 minutes at rather low temperatures between 713 K and 753 K reduces the coercive force from 2200–2500 $A{\cdot}m^{-1}$ ($= H_{as-prep}$) by a factor of 10. However, the resulting values of about 250 $A{\cdot}m^{-1}$ are still one order of magnitude higher than for the melt-spun ribbon ($H_c = 5$–$10\,A{\cdot}m^{-1}$). Annealing for longer time (10, 30 min) or at higher temperatures (753–773 K) causes even higher H_c values than for the as-milled powder. This is due to the beginning of crystallization of the initially amorphous powder. Annealing of the amorphous as-milled powder at the crystallization temperature, $T_x \approx 763$ K, for 30 minutes leads to almost complete crystallization and H_c around 7538 $A{\cdot}m^{-1}$.

3.2.3 Compacted samples

As was mentioned before, annealing of ball-milled powder leads to a reduction of H_c values which are rather high for the as-milled powder. Accordingly, one can prepare bulk samples with good soft magnetic properties, by combination of pressing and heating (hot pressing). The time and the temperature are most important parameters employed for hot pressing. Both should be kept in the region where one can prevent crystallization and prepare bulk samples with amorphous structure and good soft magnetic properties. The consolidation time is limited by the incubation time for crystallization and the consolidation temperature (T_p) is selected from the range of the supercooled liquid region. As was mentioned before, in the case of powder the supercooled liquid region becomes narrower compared to the ribbon but the stability against crystallization is still sufficient for successful consolidation of amorphous bulk specimens.

Figure 12 displays the coercivity of bulk samples as a function of the compacting temperature T_p. The characteristic temperatures T_g and T_x of the powder determined at a heating rate of $0.67\,K{\cdot}s^{-1}$ are also indicated. Coercivity values of 120–140 $A{\cdot}m^{-1}$ are found in the temperature regime of the supercooled liquid (see Table 3). The lowest coercivity of about 100 $A{\cdot}m^{-1}$ is achieved at 718 K which is the compact-

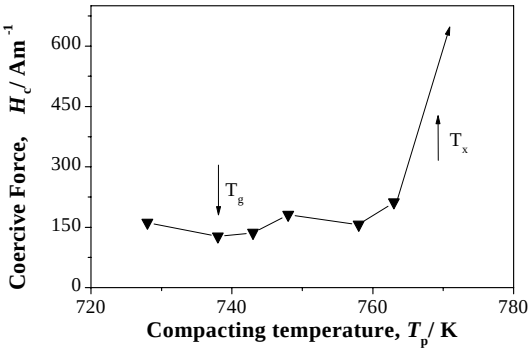

Fig. 12 Coercive force of bulk amorphous $Fe_{77}Al_{2.14}Ga_{0.86}P_{8.4}C_5B_4Si_{2.6}$ samples as a function of compacting temperature T_p. T_g and T_x are the characteristic temperatures determined from the DSC scan recorded for $Fe_{77}Al_{2.14}Ga_{0.86}P_{8.4}C_5B_4Si_{2.6}$ powder at a heating rate of 0.67 K·s^{-1}.

Table 3 Coercivity of bulk amorphous $Fe_{77}Al_{2.14}Ga_{0.86}P_{8.4}C_5B_4Si_{2.6}$ samples.

Compaction temperature, T_p/K	Coercive force, H_c/A·m^{-1}
718	106
723	127
728	161
738	127
743	136
748	181
758	156
763	212

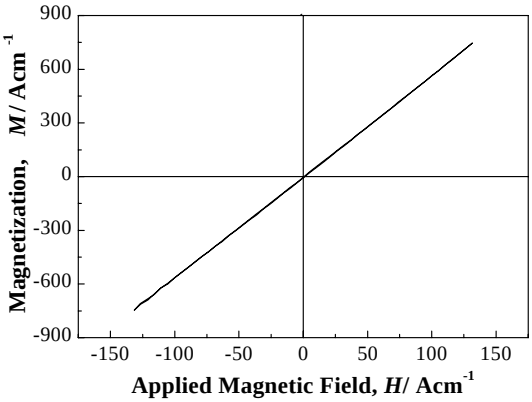

Fig. 13 M–H hysteresis loop of a bulk amorphous $Fe_{77}Al_{2.14}Ga_{0.86}P_{8.4}C_5B_4Si_{2.6}$ disc with diameter of 10 mm and height of 3 mm.

ing temperature lower then T_g (= 738 K). For higher temperatures than T_x the coercivity of bulk samples increases drastically. A similar behaviour was reported by Schlorke-de Boer *et al.*[21] for $Fe_{72}Al_5P_{11}C_6B_4Ga_2$ bulk samples with the lowest coercivity of about 30 A·m^{-1}. Figure 13 shows the hysteresis loop recorded for a compacted sample with 10 mm diameter and a height of 3 mm as a typical exemple. On can observe the hysteresis loop typical for porous material, where the mixture of nonmagnetic and magnetic particles is present.[29]

By combination of annealing and consolidation of ball-milled powder at elevated temperatures is possible to prepare Fe-based bulk amorphous specimens with different shapes and higher dimensions in comparison with the samples prepared by copper molt casting. By Inoue *et al.* was reported that the maximum thickness for glass formation of cylinders by copper mold casting is about 3 mm[16,30] and for the ring shape bulk amorphous samples: an outer diameter of 10 mm, an inner diameter of 6 mm and a thickness of 1 mm.[12]

4. Summary

Amorphous multicomponent iron-based alloys with good soft magnetic properties were obtained in bulk form either directly using copper mold casting or by hot pressing of ball-milled amorphous powder. Because for $Fe_{65.5}Cr_4Mo_4Ga_4P_{12}C_5B_{5.5}$ amorphous alloys the glass transition temperature T_g exceeds 748 K, this ferromagnetic glass is sufficiently stable for applications that require a continuous operation at high temperatures. Such alloys can be cast directly in bulk specimens if some conditions are fulfilled, *i.e.* low impurity content and proper casting temperature. The critical cooling rate is lower in comparison with classical FeB alloys, but higher than for Zr-based or Pd-based alloys.[31] This fact limits the thickness of the sample[13] and the maximum diameter of the rods obtained by copper mold casting reached 3 mm. The casting temperature plays an important role in order to obtain the amorphous phase. The presence of crystalline clusters/inclusions in the melt that can be centres for heterogeneous crystallization must be avoided. The coercivity of the fully amorphous alloy in rod form is lower than 10 A·m^{-1}. In the presence of crystalline inclusions, the H_c value increases at 62 A·m^{-1} and depend on the volume fraction and dimension of the crystalline inclusions. The existence of a small volume fraction of nanoscale crystalline precipitates is not detectable in XRD experiments in reflection configuration.

For $Fe_{77}Al_{2.14}Ga_{0.86}P_{8.4}C_5B_4Si_{2.6}$ amorphous ribbons, mechanical treatment (ball milling) of the amorphous material influences its soft magnetic properties and causes an increase of the H_c value. The significant increase of coercivity after ball milling is due to the stress field introduced by ball milling as well as to the increased oxygen content in the powders. There is a quite large coercivity relaxation of the ball-milled amorphous powders after annealing at elevated temperatures. Because of the elevated oxygen content after milling and the contribution of surface irregularities to the total coercivity,[21] a difference of about one order of magnitude is still present between the H_c values of powder and ribbon. By combination of annealing and consolidation of ball-milled powder at temperatures in the supercooled liquid region bulk amorphous specimen can be prepared with significantly larger dimensions than in the case of the mold-cast samples. The lowest coercive force obtained for the samples compacted in the supercooled liquid region is about 120 A·m^{-1}, which is about one order of magnitude higher than for the initial melt-spun amorphous ribbon.

Acknowledgements

The authors thank to Dr. Wolfgang Löser, Dr. Albert Güth, Dr. Nicole Schlorke-de Boer for stimulating discussions and to Heiko Schulze and Maik Peschel for technical assistance. This work was supported by the EU within the framework of the RTN-Network on bulk metallic glasses (HPRN-CT-2000-

00033) and partly by grant Vega 1/8305/01.

REFERENCES

1) A. Inoue and J. S. Gook: Mater. Trans., JIM **37** (1996) 32–38.
2) A. Inoue and J. S. Gook: Mater. Trans., JIM **36** (1995) 1282–1285.
3) A. Inoue: Mater. Sci. Eng. **A226–228** (1997) 357–363.
4) T. Mizushima, A. Makino and A. Inoue: IEEE Trans. Mag. **33** (1997) 3784–3784.
5) T. Mizushima, A. Makino and A. Inoue: J. Appl. Phys. **83** (1998) 6329–6331.
6) A. Inoue, A. Murakami, T. Zhang and A. Takeuchi: Mater. Trans., JIM **38** (1997) 189–196.
7) T. Mizushima, A. Makino and A. Inoue: Mater. Sci. Eng. **A226–228** (1997) 721–725.
8) A. Inoue, H. Koshiba, T. Zhang and A. Makino: Mater. Trans., JIM **38** (1997) 577–582.
9) A. Inoue and J. S. Gook: Mater. Trans., JIM **36** (1995) 1180–1183.
10) H. S. Chen: Rep. Prog. Phys. **43** (1980) 353–360.
11) N. Schlorke, J. Eckert and L. Schultz: J. Phys. D: Appl Phys. **32** (1999) 855–861.
12) T. Mizushima, K. Iskarashi, S. Yoshida, A. Makino and A. Inoue: Mater. Trans., JIM **40** (1999) 1019–1022.
13) A. Inoue, T. Zhang and A. Takeuchi: Appl. Phys. Lett. **71** (1997) 464–466.
14) A. Gebert, J. Eckert and L. Schultz: Acta Mater. **46** (1998) 5475–5482.
15) T. D. Shen and R. B. Schwarz: Appl. Phys. Lett. **75** (1999) 49–51.
16) A. Inoue, A. Makino and T. Mizushima: J. Appl. Phys. **81** (1997) 4029–4031.
17) A. Inoue, A. Kato, T. Zhang, S. G. Kim and T. Masumoto: Mater. Trans., JIM **32** (1991) 609–616.
18) Y. He, T. Shen and R. B. Schwarz: Metall. Mater. Trans. A **29** (1998) 1795–1804.
19) J. Eckert, N. Schlorke, C. A. R. T. Miranda and L. Schultz: *Synthesis and Processing of Light Weight Mettalic Materials II* ed. C. M. Ward-Close *et al*., (Warrendale: The Minerals Metals and Materials Society, 1997) pp. 383–394.
20) M. Seidel, J. Eckert, H.-D. Bauer and L. Schultz: Mater. Sci. Forum **119** (1996) 225–227.
21) N. Schlorke-de Boer, R. Schäfer, J. Eckert and L. Schultz: submitted to J. Appl. Phys.
22) N. Schlorke-de Boer: *Metallische Massivgläser auf Fe–Al–P–C–B–(Ga-) Basis und Verbundmaterialien mit Mg–Y–Cu-Glas Matrix*, Ph. D. Thesis, Technical University Dresden 2001.
23) R. B. Schwarz and Y. He: Mater. Sci. Forum **235–238** (1997) 231–240.
24) J. Eckert: Mater. Sci. Forum **3–12** (1999) 312–314.
25) J. Eckert, N. Mattern, M. Zinkevitch and M. Seidel: Mater. Trans., JIM **39** (1998) 623–632.
26) N. Schlorke, J. Eckert and L. Schultz: *Synthesis and Properties of Bulk Mettalic Mg–Y–Cu Lightweight Alloys Produced By Mechanical Alloying and Prapid Quenching*, ed. B. L. Mordike and K. U. Kainer (Werkstoff-Informationsgesellschaft: Magnesium Alloys and their Applications, Frankfurt, 1998) pp. 533–538.
27) B. Weiß and J. Eckert: Mater. Sci. Forum **343–346** (2000) 129–134.
28) Ch. Kuhrt and L. Schultz: J. Appl. Phys. **71** (1992) 1896–1900.
29) E. Kneller: *Ferromagnetismus*, (Springer-Verlag Berlin, 1962) pp. 102–105.
30) A. Inoue: Mater. Sci. Eng. **A304–306** (2001) 1–10.
31) A. Inoue and K. Hashimoto (Eds.): *Amorphous and Nano-crystalline Materials, Preparation, Properties and Applications*, (Springer, 2001) pp. 4–7.